Correlations of microstructure and mechanical properties of the ternary Sn-9wt%Zn-2wt%Cu solder alloy

Bismarck Luiz Silva[a]*, José Eduardo Spinelli[b]

[a]*Departamento de Engenharia de Materiais, Universidade Federal do Rio Grande do Norte - UFRN, 59078-970, Natal, RN, Brazil*
[b]*Departamento de Engenharia de Materiais, Universidade Federal de São Carlos - UFSCar, 13565-905, São Carlos, SP, Brazil*

The microstructure length-scales (dendritic and eutectic), morphologies and tensile properties of a ternary Sn-9wt.%Zn-2wt.%Cu alloy are compared with those of a binary eutectic Sn-9wt.%Zn alloy. The following experimental/analytical steps were performed: transient directional solidification experiments of the Sn-9wt.%Zn-2wt.%Cu alloy; measurements of secondary dendrite arm (λ_2) and interphase spacing (λ); morphology of the eutectic α-Zn phase; determination of thermal parameters such as cooling rate ($\dot{T}_L$) and their evolutions during solidification; and, finally, interrelations of microstructure *vs.* tensile properties. The addition of 2wt.%Cu causes significant refinement of the eutectic structure. Hall-Petch type experimental expressions outlined the variations of strength and ductility with both λ_2 and λ. Very fine Zn globules and needles forming the eutectic in the ternary alloy seems to cause a reversal on ductility behavior, as compared to the tendency observed for the binary Sn-9wt.%Zn alloy. Here, for the ternary Sn-9wt.%Zn-2wt.%Cu alloy ductility increases with decreasing interphase spacing.

Keywords: *Sn-Zn-Cu, solidification, microstructure.*

1. Introduction

Binary and ternary Sn-Zn-X (where X is alloying element) alloys based in the eutectic Sn-Zn composition (9wt.%Zn) are potential materials to substitute eutectic or near-eutectic Sn-Pb solder compositions[1-4]. Low melting points, suitable mechanical properties, and relatively low costs characterize the Sn-Zn alloys[5-8], when compared with others lead-free solder alloys. However, the eutectic Sn-9wt.%Zn alloy has displayed drawbacks as poor wettability and oxidation phenomenon. The addition of alloying elements, such as Ag, Cu, Bi improved such characteristics as well as mechanical properties[5-8].

It is known that the microstructural features (formation of phases, intermetallics, morphology, distribution and length-scale) may be affected by cooling thermal parameters during process (growth rate-V and cooling rate-$\dot{T}$)[9,10]. The control of these parameters during solidification process defines the final dendritic and eutectic arrangements of a certain alloy and, consequently, influences the final values of mechanical properties in the as-soldered fillets. In this context, the understanding of the roles of dendritic and eutectic arrangements in eutectic Sn-9wt.%Zn alloy with or without addition of alloying elements (X) is fundamental to achieving reliable soldered joints of Sn-Zn-X alloys.

Das et al.[5] investigated the effects 0.5wt.%Cu addition on the microstructure and tensile properties of the eutectic Sn-9wt.%Zn alloy. The microstructure of the ternary Sn-9wt.%Zn-0.5wt.%Cu alloy is formed by the Sn-rich matrix, the needle-like eutectic α-Zn, and Cu_6Sn_5/Cu_5Zn_8 intermetallics particles. El-Daly and Hammad[6,7] also informed such constituents phases for ternary Sn-Zn-Cu alloys. It was observed that the addition of 0.5%wt.Cu did not change the level of hardness of the eutectic Sn-9wt.%Zn solder alloy. On the other hand, these authors reported that the ultimate tensile strength and elongation values for the eutectic Sn-Zn alloy decreased with addition of copper, i.e., from 52MPa to 48MPa and from 62 to 38%. This reduction may be associated with the fracture mode in Sn-9wt.%Zn-0.5wt.%Cu alloy, which displayed fracture surfaces cleavage and dimple patterns. Thus, 0.5wt.%Cu containing alloy was enough to change the fracture of the eutectic Sn-9wt.%Zn alloy, going from a ductile to a complex (cleavage+dimple) fracture mode.

Rahman et al.[8] studied the effects of copper contents (0.4wt.%, 0.7wt.% and 1.0wt.%) separately added to the eutectic composition Sn-9wt.%Zn alloy, considering their microstructures and tensile properties. The microstructures for the Sn-9wt.%Zn-(0.4; 0.7; 1.0) wt. %Cu solder alloys are composed of Sn-rich matrix, α-Zn particles and primary Cu-Zn and Cu-Sn intermetallic compounds, as reported by Das et al.[5] and El-Daly and Hammad[6,7].

Lee and coauthors[11] investigated the effects of Ag and Cu separated additions in the microstructure and oxidation resistance of the eutectic Sn-9wt.%Zn solder alloy. These

authors analyzed three copper (Cu) contents, which were 1wt.%, 2wt.% and 4wt.%. They described similar microstructures to those reported by Das et al.[5] and El-Daly and Hammad[6,7]. The volumetric fraction of Cu-Zn intermetallics particles increase with increasing copper content. Considering the results of tensile properties, it can be seen that the ultimate tensile strength and yield tensile strength values slightly increase with increasing Cu content added in eutectic Sn-9wt.%Zn alloy. Strain values decrease, mainly regarding the 4wt.%Cu alloy content. Such decrease may be explained due to the higher proportion of Cu-Zn intermetallics in the microstructure of the Sn-9wt.%Zn-4wt.%Cu alloy than as compared with others Cu-modified Sn-Zn-Cu alloys. These features were confirmed with the examination of the surfaces of fracture after tensile tests with the Sn-Zn-Cu alloys. The modified alloys with smaller Cu content showed ductile fracture modes (dimple patterns), while the Sn-9wt.%Zn-4wt.%Cu alloy displayed a mixture fracture mode constituted by cleavage and dimple patterns, where cleavage regions were directly associated with the Cu-Zn intermetallic compounds (IMCs).

El-Daly and Hammad[7] performed tensile mechanical tests in the Sn-9wt.%Zn and Sn-9wt.%Zn-0.7wt.%Cu alloys, varying the strain rate. It can be seen that the ultimate tensile strength and yield tensile strength values slightly increase with increasing of strain rate for both alloys, with the Cu-modified alloy slightly having higher values than for eutectic Sn-9wt.%Zn solder alloy. The total elongation did not showed tendency with the strain rate variation in both examined alloys.

By examining the aforementioned findings concerning microstructure and mechanical properties in Sn-Zn-Cu[5-8,11], correlations between the local length scales of the microstructure of the Sn-9Zn-Cu alloys, the formed IMCs and tensile properties are still undetermined in literature.

In order to gain insight into mechanical behavior of the ternary Sn-9wt.%Zn-2wt.%Cu alloy, experimental interrelations of ultimate-σ_u/yield-σ_y tensile strengths and elongation-δ with the microstructural parameters λ_2 and λ have been proposed. Experimental growth relations showing the dependence of the microstructure on the cooling rate-$\dot{T}$ were also determined. The experimental findings for the ternary Sn-9wt.%Zn-2wt.%Cu alloy are compared to those previously reported for the eutectic Sn-9wt.%Zn.

2. Experimental Procedure

2.1 Directionally solidified casting

The ternary Sn-9wt.%Zn-2wt.%Cu alloy has been assessed. A water-cooled solidification setup was used so that the directionally solidified samples could be produced as can be seen in details in Figure 1. This system promotes a vertical upward solidification. The heat is removed through the bottom of the casting while the solid alloy grows from the bottom to the top, as can be observed in Figure 1.
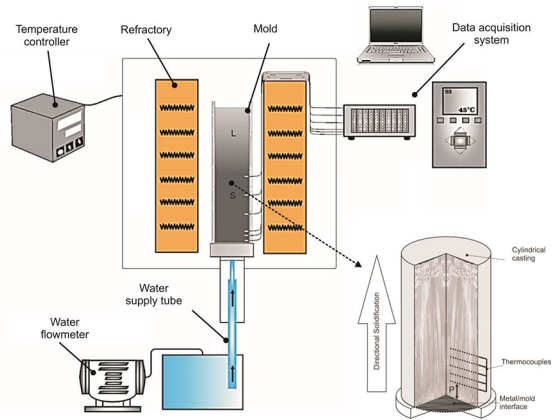
Figure 1. Vertical upward directional solidification casting assembly and its devices used to produce the directionally solidified Sn-9Zn-2Cu alloy casting.

A water-cooled bottom made of low carbon steel (SAE 1020-3mm thick) was used to close the system so that the vertical upward growth of the alloy starts from its surface. A stainless steel split mold was used having the following dimensions: 60 mm of internal diameter, 157mm of height and 5mm of wall thickness. The application of a layer of insulating alumina-silica ceramics in inner split mold surface minimized heat losses.

The following procedures were performed for the alloy: firstly, the alloy is melted *in situ* by radial electrical wiring positioned around a split stainless-steel mold. Secondly, when the melt temperature is about 10% above either the *liquidus* temperature, the electric heaters are disconnected and at the same time the water flow at the bottom of the container is started, which allows the onset of solidification. Finally, the evolution of temperatures along the length of the casting was measured, was monitored by fine type J thermocouples (0.2 mm diameter wire), placed in the geometrical center of the cylindrical mold cavity, but in various different relative positions along its length. The temperature-time records from the data acquisition system (see Figure 1) were stored with a view to permitting the cooling rates ($\dot{T}$) to be determined. $\dot{T}$ was determined along the casting length, by considering the thermal data recorded immediately after the passage of the *liquidus* front by each thermocouple.

2.2 Analytical tools

Metallographic analysis was performed to reveal the microstructural and morphological details of the Sn-Zn-Cu alloy, using grinding and polishing steps combined with the etchant 2mL HC*l*, 10mL FeC*l*$_3$ and 100mL H$_2$O. Various selected transverse cross (perpendicular to growth direction) and longitudinal (parallel to the growth direction) sections of samples along the casting length were examined.

Micrographs were obtained using a light microscope with a coupled optical image processing system Olympus, GX51 (Olympus Co., Japan) and using a Field Emission Gun (FEG) - Scanning Electron Microscope SEM-EDS

FEI (Inspect S50L). The intercept method was employed to determine both the secondary dendritic arm spacing (λ_2) and the interphase spacing (λ) on longitudinal and transverse sections of the DS castings, respectively[12].

Transverse specimens extracted from different positions along the length of the DS castings were prepared according to specifications of the ASTM Standard E 8M/04 and tested in an Instron 5500R machine at a strain rate of about 3×10^{-3} s^{-1}. The ultimate/yield tensile strengths and elongation-to-fracture have been determined and related to average microstructural spacings. Four specimens of each selected position were tested so that reproducibility may be assured. To guarantee a broad span of measurements, several specimens were extracted from the water-cooled bottom of the casting, as can be seen in Figure 2. The relative positions of interest are also shown in Figure 2.
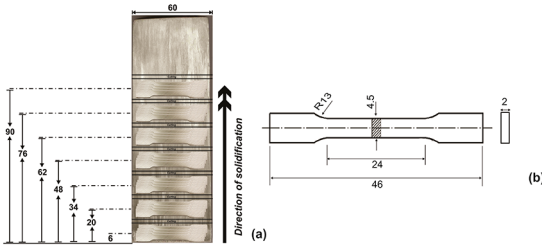
Figure 2. (a) Schematic representation of relative positions in Sn-9wt.%Zn-2wt.%Cu solder alloy casting from where the specimens for tensile tests were extracted and (b) details of the geometrical dimensions of tensile specimens (dimensions in mm).

Images of the fracture surfaces were obtained using two Scanning Electron Microscopes (SEM-EDS): Hitachi (TM3000 model) and Zeiss (Auriga model). After the tensile tests, the two parts of each specimen were properly preserved and then taken for analysis by SEM.

The X-ray diffraction (XRD) patterns of the phases formed in the Sn-9wt.%Zn-2wt.%Cu solder alloy examined have been acquired by a Siemens D5000 diffractometer with a 2-theta range from 20° to 90°, CuKα radiation and a wavelength, λ, of 0.15406 nm. The XRD patterns were assessed at a scan speed of 2°/min.

3. Results and Discussion

As the microstructure of the Sn-9wt.%Zn-2wt.%Cu solder alloy solder alloy is formed by a fully dendritic arrangement, Figure 3 shows the evolution of secondary (λ_2) dendritic arm spacings as a function of the cooling rate ($\dot{T}_L$). The points in the graphs represent the average microstructural spacing experimentally measured along with its standard variation. The line represents the empirical power law fitted to the experimental points for the dendritic growth of the Sn-9wt.%Zn-2wt.%Cu solder alloy. A -1/3 power law

characterizes the secondary dendrite arm spacings variations with cooling rate. The results establish that strong variation
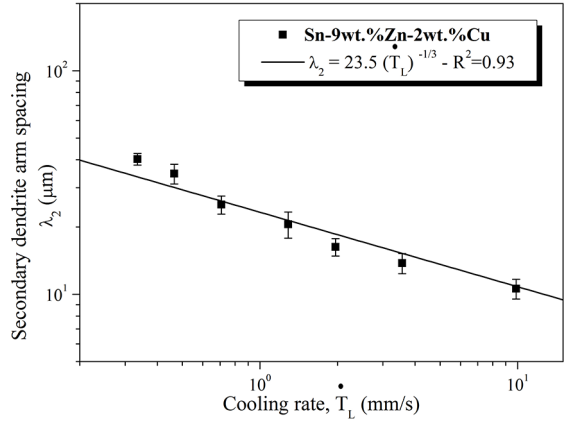
Figure 3. Secondary dendritic spacing (λ_2) as a function of cooling rate ($\dot{T}_L$) for the Sn-9wt.%Zn-2wt.%Cu solder alloy. R^2 is the coefficient of determination.

in the microstructural spacing (λ_2) is achieved because of the variation in cooling rate during solidification.

The exponent typically employed to represent λ_2 variations with solidification kinetics is -2/3. This is used to describe the growth of secondary dendritic arms with V_L, being reported in the form of a theoretical model proposed by Bouchard and Kirkaldy - BK[13]. The BK model can be represented by the expression λ_2=constant x $V_L^{-2/3}$. However, it is worth noting that the cooling rate ($\dot{T}$) for transient solidification conditions is represented by the following expression: $\dot{T}_L$ = constant x V_L^2[14,15]. If such expression is inserted into that proposed by Bouchard and Kirkaldy, λ_2 may be related to the cooling rate according to a power function exponent of -1/3. This is in agreement with the experimental growth law derived in Figure 3.

Garcia[16] stated the following experimental power equations to represent variations in λ_2 for hypoeutectic Sn-4wt.%Zn and hypereutectic Sn-12wt.%Zn alloys: λ_2=32($\dot{T}_L$)$^{-0.55}$ and λ_2=43($\dot{T}_L$)$^{-0.55}$, respectively. Comparing those experimental results with the expression derived in the present investigation λ_2=23.5($\dot{T}_L$)$^{-1/3}$, one can affirm that λ_2 in the ternary Sn-Zn-Cu alloy is generally smaller than that characterizing hypoeutectic and hypereutectic compositions.
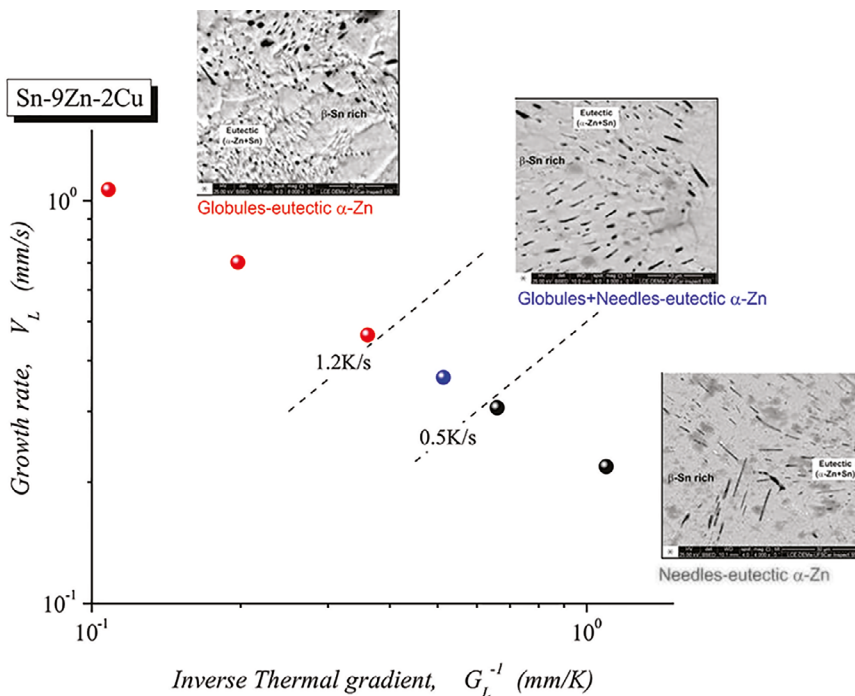
Through the thermal data acquired during the directional solidification experiments, plots of position (P), from the metal/mold interface, against the corresponding time (t_L) of the *liquidus* isotherm passing by each thermocouple were generated, i.e., P=f(t_L). This function was thus derived as a function of time resulting in another function as follows: V_L=f(t_L). $\dot{T}_L$ can be generally defined as $G_L \times V_L$.

Figure 4 shows a G_L-V_L map describing the variation of the eutectic α-Zn morphology with cooling rate for

the ternary Sn-Zn-Cu alloy. Considering that the as-cast microstructures are arranged by the Sn-rich dendrites and the primary Cu_5Zn_8 intermetallic particles, different shapes of the eutectic mixture Sn+α-Zn were observed, which were *globular-like* (closer to the bottom of the casting), mixture of *globular-like and needle-like* (intermediate positions) and *needle-like* (closer to the top of the casting).

It can be seen that high $\dot{T}_L$ and V_L (low G_L^{-1}) induce globular formation. As V decreases, the morphology of eutectic Zn becomes less refined, transitioning from globules to needles. A mixture of globules and needles is also observed. This seems to be a result of the coalescence of globules giving rise to needles, which justifies a narrow region of mixed globules and needles. The critical cooling rate for the formation of globular Zn is found to be 1.2ºC/s, while cooling rates lower than 0.5ºC/s permitted the formation of needles.

Based on the SEM images, measurements of interphase spacings were performed along the DS Sn-Zn-Cu alloy casting. The average interphase spacings (λ) with their standard deviations are shown in Figure 5. The average λ values varied from 1.2 µm to 3.6 µm. In contrast to that, the λ values representing globules diameter or needles width for the Sn-9wt.%Zn alloy reported by Osório et al.[1,2] varied from 5.0 µm to 16 µm. Hence, the addition of Cu is able to reduce the range of λ values in around 4 times, which proves a considerable refinement effect for the eutectic structure.

The exponent -1/2 is that suggested by Jackson and Hunt for growth of regular eutectics[17] considering the variation of λ against growth rate. Based on this traditional model and for the same reasons given before in the case of $λ_2$ evolution against cooling rate, considering that $\dot{T}$ = constant x V^2, a power function exponent of -1/4 may represent the variation of λ *vs.* cooling rate. This agrees with the power function law derived in Figure 5.

Figure 6 shows the X-ray diffractograms obtained for the Sn-9wt.%Zn-2wt.%Cu solder alloy at two different positions from the bottom of the casting. Samples that experienced very distinct cooling rates were chosen. Thus, it is possible to examine the impacts of cooling rate on the phases forming in the microstructure. The X-ray diffractograms show the presence of peaks associated with the Cu_5Zn_8 IMC, Sn-rich and Zn-rich phases. Both cooling conditions samples, i.e., 0.2ºC/s and 9.9ºC/s show the same set of phases according to the XRD.

The darker particles in the SEM microstructures of Figure 7 are the Cu_5Zn_8. As can be observed in Figure 7 through these microstructures, different sizes of Cu_5Zn_8 may happen depending on the position examined from the cooled surface of the DS Sn-Zn-Cu alloy casting. This means that the sizes vary from smaller at positions closer to the bottom of the casting, to larger IMCs for positions closer to the top of the casting. The Cu_5Zn_8 phase as well
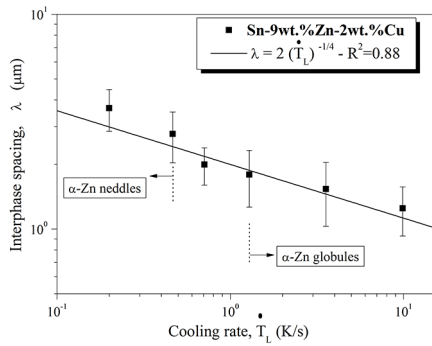

Figure 4. Diagram showing a map in G-V space with the eutectic Zn morphology and cooling rate based on DS results for the ternary Sn-9wt.%Zn-2wt.%Cu solder alloy.
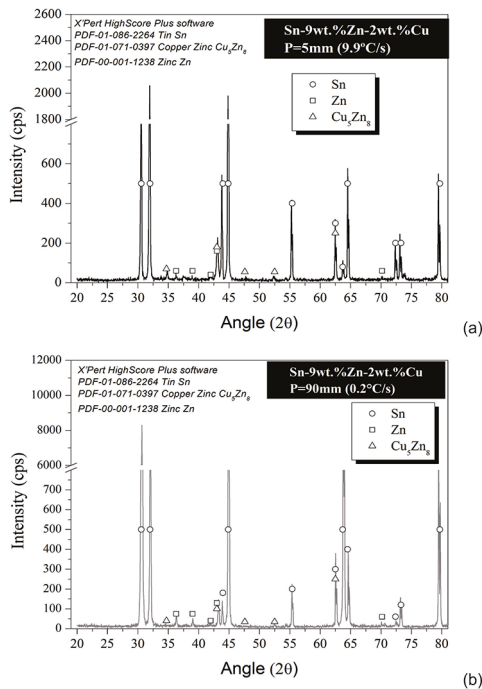
Figure 5. Interphase spacing as a function of cooling rate ($\dot{T}_L$) for the Sn-9wt.%Zn-2wt.%Cu solder alloy. R^2 is the coefficient of determination.

Figure 6. X-ray diffraction (XRD) patterns of the Sn-9wt.%Zn-2wt.%Cu solder alloy for two positions (a) P=5mm and (b) P=90mm along the length of the DS casting.

as the dendritic arrangement were observed all across the longitudinal direction of the DS Sn-Zn-Cu alloy casting.

Figure 8 depicts typical stress-strain curves of the as-cast Sn-9wt.%Zn-2wt.%Cu solder alloy specimens extracted from three different positions along the casting length (i.e.: P=6mm, P=48mm and P=90mm from the bottom of the DS casting). It can be seen that both tensile stress and strain decrease for positions farther from the cooled surface of the casting. The ultimate tensile strength associated with the position 6mm was around 40% higher than that determined

for the position 90mm, while the elongation-to-fracture was varied around 140% between such positions.

Figure 9 and Figure 10 show the results regarding the three parameters (ultimate tensile strength-σ_u, yield tensile strength-σ_y and elongation to fracture-δ) as determined from the tensile mechanical tests of the Sn-9wt.%Zn-2wt.%Cu alloy specimens. The secondary dendritic spacing and interphase spacing were considered as the varied microstructural parameters in the abscissas of the plots in Figure 9 and Figure 10, respectively. The experimental scatters matched Hall-Petch type correlations. Therefore, $\lambda^{-1/2}$ and $\lambda_2^{-1/2}$ defined the X-coordinates.

It can be seen that decrease in both the secondary dendritic spacing and the interphase spacing of the Sn-Zn-Cu alloy are associated with increase in σ_u, σ_y and δ. The interdendritic regions of the Sn-9wt.%Zn-2wt.%Cu alloy are composed of a eutectic mixture Sn+α-Zn, with the reinforcing phase being α-Zn phase[18,19]. Smaller λ_2 and λ values induce a more homogeneous distribution of the α-Zn particles in the eutectic regions, improving the mechanical properties (σ_u, σ_y and δ) of the examined alloy, as can be seen in Figure 9 and Figure 10. The load transfer from Sn-rich matrix to the rigid eutectic phase seems to cause the contribution to the strength of this alloy.

Furthermore, by examining the SEM images in Figure 4, it can be seen that the α-Zn particles has globular-like type morphology closer to the bottom of the casting, i.e., for specimens characterized by finer λ and λ_2. This morphology seems to contribute in increasing both mechanical strength and ductility. Also for positions closer to the bottom of the casting, smaller primary Cu_5Zn_8 phase developed (Figure 7). These particles in those regions are evenly distributed than those characterizing the microstructures typically observed for farther positons along the casting length. Such hard primary intermetallics may contribute when properly distributed in the final microstructure, promoting increase in σ_u, σ_y and δ.

In order to establish a comparison between the Hall-Petch type correlations of the eutectic Sn-9wt.%Zn alloy[2] and the ternary Sn-9wt.%Zn-2wt.%Cu solder, experimental tendencies of the binary alloy were included in Figure 10 (dotted lines).

The addition of 2wt.%Cu has deleterious effects on both the ultimate tensile strength, and the yield tensile strength, as compared to those representing the Sn-9wt.%Zn alloy. It is very reasonable to expect that coarse Cu_5Zn_8 primary intermetallics formed in the microstructure of the Cu-modified alloy could result in decrease the strength. As previously stated by some authors[6,7,11], the presence of Cu-Zn intermetallics depreciate the tensile strength and ductility of ternary Sn-Zn-Cu alloys.

The Cu_5Zn_8 IMCs found in the microstructure of Sn-Zn-Cu alloys may act as preferential points for fracture, reducing the tensile strength. This explanation is in agreement with
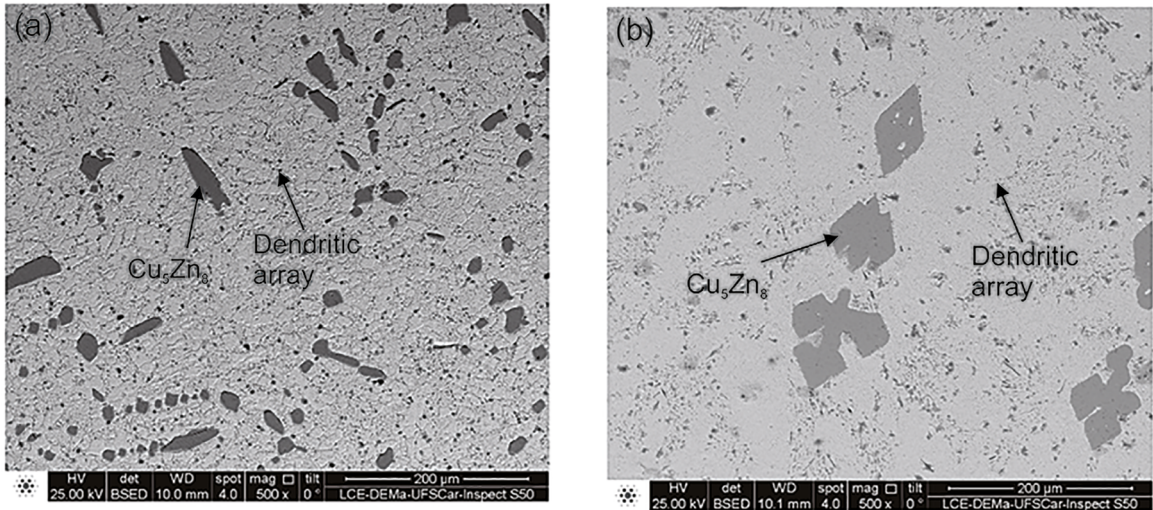
Figure 7. Scanning electron microscopy (SEM) microstructures of transverse sections detailing the primary IMC for the Sn-9wt.%Zn-2wt.%Cu solder alloy. For positions (a) P=5mm and (b) P=70mm along the length of the DS casting.
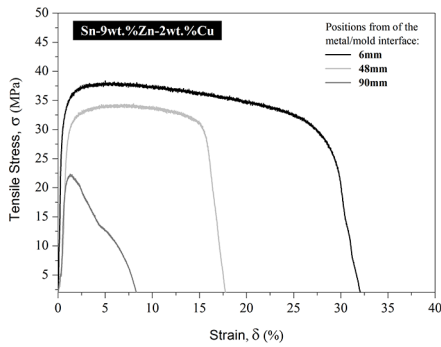

Figure 8. Tensile stress-strain curves corresponding to the specimens extracted at the positions 6mm, 84mm and 90mm from the cooled surface of the ternary Sn-9wt.%Zn-2wt.%Cu alloy.

the present results that show very clearly the decline in the alloy strength. However, opposite tendencies were noted for the variation in ductility as compared to those established for the strength plots.

Even though δ values of the Sn-9wt.%Zn (dotted line) tends to decrease with decreasing λ, a substantial reversal of this trend may happen if considered the results of the Cu-modified alloy, resulting in a "V-shaped" whole tendency. The reverse trend is shown to be associated with $\lambda^{-1/2}$ higher than 0.56, i.e., for microstructures formed by very fine eutectic Zn globules or mixture of Zn globules + Zn needles, also very refined. These morphologies are related to fast cooling conditions during solidification. Thus, a remarkable recovery in ductility took place because of the mentioned eutectic refinement within the Sn-9wt.%Zn-2wt.%Cu alloy.
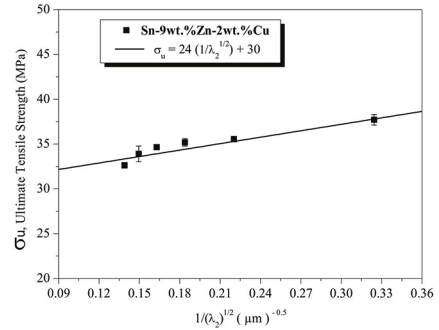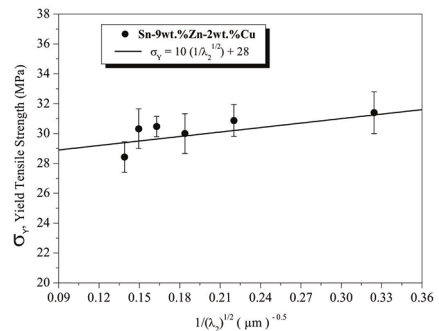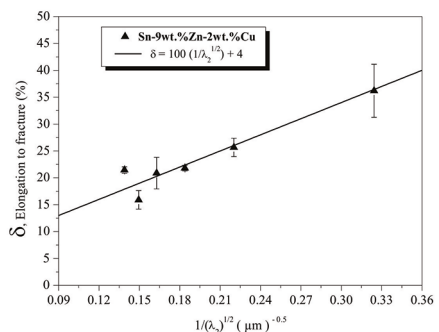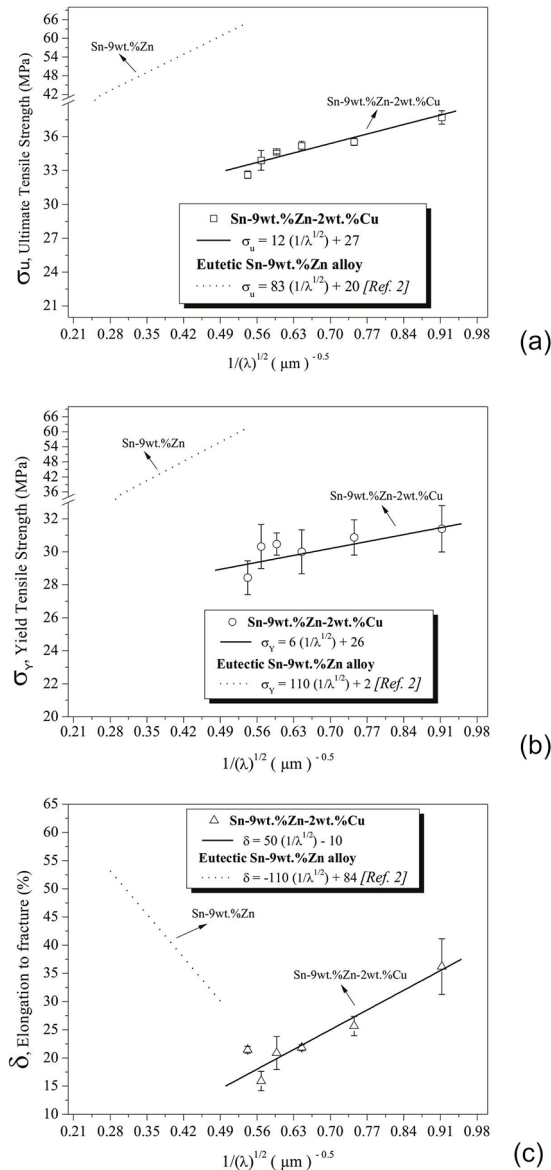

Figure 9. (a) Ultimate tensile strength, (b) yield tensile strength and (c) elongation-to-fracture as a function of the secondary dendrite arm spacing, λ_2, for the Sn-9wt.%Zn-2wt.%Cu solder

Figure 10. (a) Ultimate tensile strength, (b) yield tensile strength and (c) elongation-to-fracture as a function of the interphase spacing, λ, for the Sn-9wt.%Zn-2wt.%Cu solder alloy.

Smaller sizes of the eutectic phases induce an increase in contact area between them. Under load conditions, this seems to increase sliding potentials between the interfaces of the adjacent phases. Such interactions may occur especially on necking stage, thus providing an increase on the ductility. According to Dieter[20], globulized reinforcing particles play an important role on ductilizing metals. This shape can assist the movement of the dislocation lines inducing better ductility, as compared to others shapes.

Das et al.[5] studied the effects of a small addition of Cu on the microstructure and on the tensile properties of the eutectic Sn-9wt.%Zn alloy. For a ternary Sn-9wt.%Zn-0.5wt.%Cu alloy, strength and ductility of 48MPa and 38%, respectively, were attained. Such values are close to those found for the specimens associated with fast solidification, i.e., smaller λ and λ_2, despite much higher Cu content.

Rahman and co-authors[8] reported tensile strength and ductility of 42MPa and 38% for the ternary Sn-9wt.%Zn-1wt.%Cu alloy. Lee et al.[11] reported superior strength for the Sn-9wt.%Zn-2wt.%Cu alloy, as compared to the present findings. In this case, the measured cooling rate during the production of the castings was 40°C/s. Such cooling condition is around 4 times more severe than the fast cooled sample examined in the present study. Consequently, one could expect a finer eutectic structure, which explains the superior strength.

Figure 11 shows the SEM fracture surfaces of the Sn-9wt.%Zn-2wt.%Cu solder alloy for three different positions along the casting length after tensile mechanical tests. In all specimens similar characteristics are observed, i.e., regions with typical ductile and fragile fracture modes may be noticed. Dimpled and cleavage patterns can be observed in all fractographies. In the brittle regions the fracture may occur throughout the particle and is directly related with the presence of primary Cu_5Zn_8 intermetallics compounds in the microstructure of the Sn-9wt.%Zn-2wt.%Cu alloy, while ductile regions are associated with either the Sn-rich dendrites or the Sn+α-Zn eutectics. This means that void nucleation seems to happen from both mentioned features in the microstructure.

River markings, characteristic structure of the cleavage fracture mechanism[21], have been found throughout the Cu_5Zn_8 IMCs. The failure modes are the same for the three positions along the DS casting length as can be seen in the Figure 11. Das and co-authors[5], Rahman et al.[8], Lee et al.[11] and El-Daly and Hammad[7] described similar fracture mechanisms for ternary Sn-Zn-Cu alloys.

Very refined dimples are perfectly consistent with eutectic mixture on the alloy microstructure, as can be seen in the detail of Figure 11 (see the inset fractography shown at upper right for P=6mm). Sn-rich triple points, also known as crows' feet marks, can also be noted in Figure 11. This is due the local ductile behavior indicating flow of the material until local cross-sectional area attains zero, provoking disconnection of the parts. This is mainly related to the necking step during load. This kind of disconnection of the parts is more noticeable for the fractures referring to the position 6mm, in which by very fine eutectic Zn globules were observed. Thus, higher ductility (36.2%) was attained accordingly.
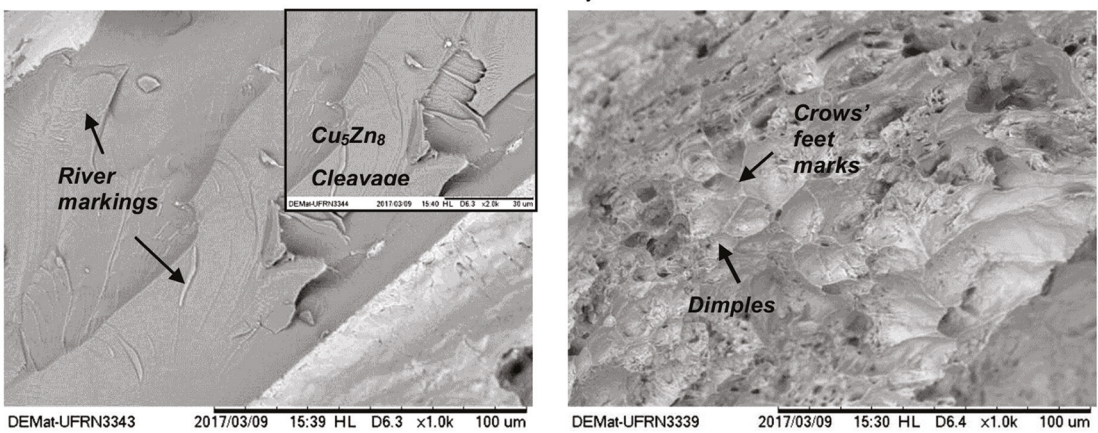
a) P=6mm: σ_u=37.7MPa; σ_y=31.4MPa e δ=36.2%

b) P=48mm: σ_u=34.7MPa; σ_y=30.5MPa e δ=20.9 %
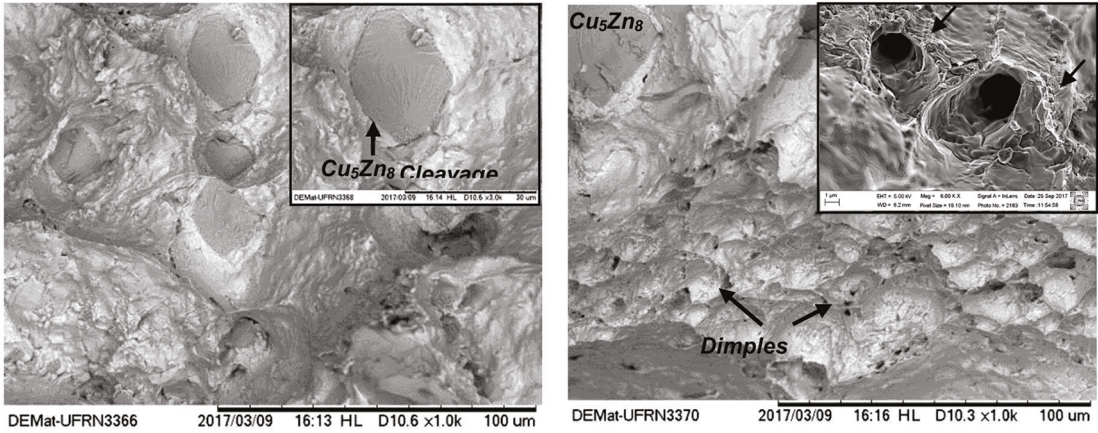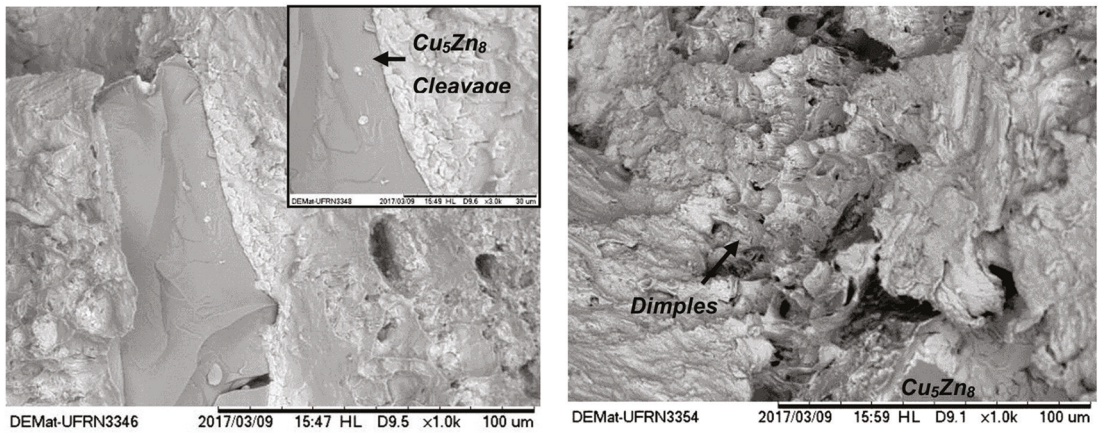
c) P=90mm: σ_u=21.6MPa; σ_y=20.0MPa e δ=12.4%

Figure 11. SEM fracture surfaces of the Sn-9wt.%Zn-2wt.%Cu solder alloy corresponding to tensile specimens extracted at different positions (i.e., a) 6mm, b) 48mm and c) 90mm) from the cooled surface of the DS casting.

4. Conclusions

From the findings achieved in this investigation, the following conclusions can be drawn:

1. Microstructures development (i.e. scale and morphology) during directional solidification of the Sn-9Zn-2Cu solder alloy was analyzed as a function of cooling rate. The solidification path has been mapped out. Zn morphology is found to vary from elongated/needles to round/globular as the cooling rate increases. Cooling rates higher than 1.2ºC/s propitiate a globulized eutectic structure to prevail.

2. The addition of Cu in Sn-9Zn is able to reduce the range of λ (interphase spacing) values in around 4 times, which proves a considerable refinement effect for the eutectic structure.

3. Both ductile and fragile fracture modes have been noticed by examining the fracture surfaces of the ternary Sn-9Zn-2Cu alloy specimens. Very refined dimples and crows' feet marks are noted. These features are perfectly consistent with the ductility behavior observed for the specimens associated with faster solidification, i.e., smaller λ and λ_2.

4. The present findings suggests that, by making appropriate choices of the solidification parameters, microstructures of Sn-9Zn-2Cu alloy can be controlled so that the desired fine globular Zn morphology is obtained. Consequently, an improved ductility level may be attained.

5. Acknowledgements

6. References

1. Garcia LR, Osório WR, Peixoto LC, Garcia A. Mechanical properties of Sn-Zn lead-free solder alloys based on the microstructure array. *Materials Characterization*. 2010;61(2):212-220.

2. Osório WR, Peixoto LC, Garcia LR, Mangelinck-Noël N, Garcia A. Microstructure and mechanical properties of Sn-Bi, Sn-Ag and Sn-Zn lead-free solder alloys. *Journal of Alloys and Compounds*. 2013;572:97-106.

3. Islam MN, Chan YC, Rizvi MJ, Jillek W. Investigations of interfacial reactions of Sn-Zn based and Sn-Ag-Cu lead-free solder alloys as replacement for Sn-Pb solder. *Journal of Alloys and Compounds*. 2005;400(1-2):136-144.

4. Suganuma K, Niihara K, Shoutoku T, Nakamura Y. Wetting and interface microstructure between Sn-Zn binary alloys and Cu. *Journal of Materials Research*. 1998;13(10):2859-2865.

5. Das SK, Sharif A, Chan YC, Wong NB, Yung WKC. Influence of small amount of Al and Cu on the microstructure, microhardness and tensile properties of Sn-9Zn binary eutectic solder alloy. *Journal of Alloys and Compounds*. 2009;481(1-2):167-172.

6. El-Daly AA, Hammad AE. Elastic properties and thermal behavior of Sn-Zn based lead-free solder alloys. *Journal of Alloys and Compounds*. 2010;505(2):793-800.

7. El-Daly AA, Hammad AE. Effects of small addition of Ag and/or Cu on the microstructure and properties of Sn-9Zn lead-free solders. *Materials Science and Engineering: A*. 2010;527(20):5212-5219.

8. Rahman M, Sharif A, Ahmed M. Effect of various amount of Cu on the thermal and mechanical behavior of Sn-9Zn eutectic Pb-free solder alloy. In: *Proceedings of the International Conference on Mechanical Engineering 2009 (ICME2009)*; 2009 Dec 26-28; Dhaka, Bangladesh. 2009. p. 1-6.

9. Kurz W, Fisher DJ. *Fundamentals of Solidification*. Zurich: Trans Tech Publications; 1992.

10. Garcia A. *Solidificação: Fundamentos e Aplicações*. Campinas: Editora Unicamp; 2011.

11. Lee JE, Kim KS, Inoue M, Jiang J, Suganuma K. Effects of Ag and Cu addition on microstructural properties and oxidation resistance of Sn-Zn eutectic alloy. *Journal of Alloys and Compounds*. 2008;454(1-2):310-320.

12. Gündüz M, Cadirli E. Directional solidification of aluminium-copper alloys. *Materials Science and Engineering: A*. 2002;327(2):167-185.

13. Silva BL, Silva VCE, Garcia A, Spinelli JE. Effects of Solidification Thermal Parameters on Microstructure and Mechanical Properties of Sn-Bi Solder Alloys. *Journal of Electronic Materials*. 2017;46(3):1754-1769.

14. Garcia A, Prates M. Mathematical model for the unidirectional solidification of metals: I. cooled molds. *Metallurgical Transactions B*. 1978;9(3):449-457.

15. Garcia A, Clyne TW, Prates M. Mathematical model for the unidirectional solidification of metals: II. Massive molds. *Metallurgical Transactions B*. 1979;10(1):85-92.

16. Garcia LR. *Microestrutura de Solidificação e Propriedades Mecânicas de Ligas Sn-Zn para Soldagem e Recobrimento de Superfícies*. [Thesis]. Campinas: State University of Campinas (UNICAMP); 2008. 148 f.

17. Jackson KA, Hunt JD. Lamellar and Rod Eutectic Growth. *Transactions of the Metallurgical Society of AIME*. 1966;236:1129-1142.

18. El-Daly AA, Hammad AE, Al-Ganainy GA, Ibrahiem AA. Enhancing mechanical response of hypoeutectic Sn-6.5Zn solder alloy using Ni and Sb additions. *Materials & Design (1980-2015)*. 2013;52:966-973.

19. Silva BL, Reyes RV, Garcia A, Spinelli JE. Dendritic Growth, Eutectic Features and Their Effects on Hardness of a Ternary Sn-Zn-Cu Solder Alloy. *Acta Metallurgica Sinica (English Letters)*. 2017;30(6):528-540.

20. Dieter GE. *Mechanical Metallurgy*. London: McGraw-Hill; 1988.

21. Meyers M, Chawla K. *Mechanical Behavior of Materials*. Cambridge: Cambridge University Press; 2009.